Competition of Superconducting Phenomena and Kondo Screening at the Nanoscale

K. J. Franke, *et al.*

Science **332**, 940 (2011);
DOI: 10.1126/science.1202204

Figure 4 summarizes the phase behavior of the SLs with $N = 2$, which undergo a sequence of two sharp, collective electronic phase transitions upon cooling. We have provided strong evidence that the two transitions correspond to the onset of charge and spin order. By showing that the $N = 4$ counterparts remain uniformly metallic and paramagnetic at all temperatures, we have demonstrated full dimensionality control of these collective instabilities. The higher propensity toward charge and spin order in the 2D systems probably reflects enhanced nesting of the $LaNiO_3$ Fermi surface. The phase behavior is qualitatively similar to the one observed in bulk $RNiO_3$ with small radius of the R anions, which results from bandwidth narrowing due to rotation of NiO_6 octahedra, but the transition temperatures and the order parameters are substantially lower, probably because of the reduced dimensionality. Because the transitions occur in the $N = 2$ SLs, regardless of whether the substrate-induced strain is compressive (Fig. 1B) or tensile (Fig. 1C), structural parameters such as rotation and elongation of the NiO_6 octahedra can be ruled out as primary driving forces. We note, however, that the infrared conductivity is higher (Fig. 2, A and B) and the transition temperatures are lower (Fig. 4) in the $N = 2$ SL grown under tensile strain. The more metallic response of these SLs, compared with those grown under compressive strain, may reflect a widening of the Ni 3*d*-electron bandwidth and/or an enhanced occupation of the Ni $d_{x^2-y^2}$ orbital polarized parallel to the $LaNiO_3$ layers. A small orbital polarization was indeed detected by soft x-ray reflectometry in our superlattices (*17*). This indicates further opportunities for orbital control of the collective phase behavior of the nickelates, which may enable experimental tests of theories predicting high-temperature superconductivity (*18*, *19*) or multiferroicity (*20*) in these systems.

References and Notes

1. E. Dagotto, *Science* **309**, 257 (2005).
2. J. Mannhart, D. G. Schlom, *Science* **327**, 1607 (2010).
3. M. Imada, A. Fujimori, Y. Tokura, *Rev. Mod. Phys.* **70**, 1039 (1998).
4. R. Eguchi *et al.*, *Phys. Rev. B* **79**, 115122 (2009).
5. I. I. Mazin *et al.*, *Phys. Rev. Lett.* **98**, 176406 (2007).
6. J. L. García-Muñoz, M. A. G. Aranda, J. A. Alonso, M. J. Martínez-Lope, *Phys. Rev. B* **79**, 134432 (2009).
7. V. Scagnoli *et al.*, *Phys. Rev. B* **73**, 100409(R) (2006).
8. V. Scagnoli *et al.*, *Phys. Rev. B* **77**, 115138 (2008).
9. H.-U. Habermeier, *Mater. Today* **10**, 34 (2007).
10. Materials and methods are available as supporting materials on *Science* Online.
11. J. W. Freeland *et al.*, *Phys. Rev. B* **81**, 094414 (2010).
12. X. Q. Xu, J. L. Peng, Z. Y. Li, H. L. Ju, R. L. Greene, *Phys. Rev. B* **48**, 1112 (1993).
13. T. Katsufuji, Y. Okimoto, T. Arima, Y. Tokura, J. B. Torrance, *Phys. Rev. B* **51**, 4830 (1995).
14. T. Proksch *et al.*, *Nucl. Instrum. Methods Phys. Res. A* **595**, 317 (2008).
15. J. L. García-Muñoz, P. Lacorre, R. Cywinski, *Phys. Rev. B* **51**, 15197 (1995).
16. J. L. García-Muñoz *et al.*, *Physica B* **374–375**, 87 (2006).
17. E. Benckiser *et al.*, *Nat. Mater.* **10**, 189 (2011).
18. J. Chaloupka, G. Khaliullin, *Phys. Rev. Lett.* **100**, 016404 (2008).
19. P. Hansmann *et al.*, *Phys. Rev. Lett.* **103**, 016401 (2009).
20. G. Giovannetti, S. Kumar, D. Khomskii, S. Picozzi, J. van den Brink, *Phys. Rev. Lett.* **103**, 156401 (2009).

Acknowledgments: We thank Y.-L. Mathis and R. Weigel for support at the infrared IR1 and Max-Planck-Institut für Metallforschung x-ray beamlines of the synchrotron facility Angström Quelle Karlsruhe (ANKA) at the Karlsruhe Institute of Technology. We thank G. Khaliullin and O. K. Andersen for discussions, W. Sigle and P. A. van Aken for support and discussions of transmission EM results, A. Szökefalvi-Nagy for x-ray software support, and G. Logvenov for support in sample growth and characterization. This work was supported by the Deutsche Forschungsgemeinschaft, grant TRR80, project C1. V.K.M. and C.B. were supported by the Schweizerische Nationalfonds via grants 200020-129484 and NCCR-MaNEP.

Supporting Online Material

www.sciencemag.org/cgi/content/full/332/6032/937/DC1
Materials and Methods
Figs. S1 to S10
Table S1
References

10 January 2011; accepted 21 March 2011
10.1126/science.1202647

Competition of Superconducting Phenomena and Kondo Screening at the Nanoscale

K. J. Franke,* G. Schulze, J. I. Pascual

Magnetic and superconducting interactions couple electrons together to form complex states of matter. We show that, at the atomic scale, both types of interactions can coexist and compete to influence the ground state of a localized magnetic moment. Local spectroscopy at 4.5 kelvin shows that the spin-1 system formed by manganese-phthalocyanine (MnPc) adsorbed on Pb(111) can lie in two different magnetic ground states. These are determined by the balance between Kondo screening and superconducting pair-breaking interactions. Both ground states alternate at nanometer length scales to form a Moiré-like superstructure. The quantum phase transition connecting the two (singlet and doublet) ground states is thus tuned by small changes in the molecule-lead interaction.

When a magnetic atom or molecule is adsorbed on the surface of a superconductor, its magnetic moment can interact with itinerant electrons (with spin s = 1/2) and with Cooper pairs (s = 0). Normal-state electrons tend to screen the local magnetic moment and form a many-particle ground state with a total spin S = 0. A fingerprint of this so-called Kondo effect (*1*) is a resonance at the Fermi level, whose width reflects the energy scale of the magnetic coupling. The magnetic impurity can also weaken the local coherence of the superconducting state by the creation of spin-polarized bound states in its proximity (*2–4*). They appear as narrow resonances inside the superconducting energy gap (*5–10*). The energy position of these intragap states reflects the pair-breaking exchange interaction strength of the magnetic impurity with Coopers pairs (*9*, *10*).

These interactions compete to produce two different magnetic ground states depending on their relative strength. A Kondo singlet is formed if the screening energy scale is larger than the pairing energy of the Cooper quasiparticles, that is, $k_B \cdot T_K >> \Delta$, where k_B (the Boltzmann constant), T_K (the Kondo temperature) determines the energy scale of the screening, and the order parameter Δ governs the superconductor pairing interaction. When $k_B \cdot T_K << \Delta$, the opening of the superconducting energy gap reduces the density of normal electrons available for screening, and the Kondo effect is incomplete (*11*). The poorly screened magnetic impurity creates bound quasiparticle states that locally reduce the pairing strength of the superconducting quasiparticles and drive the system into a magnetic ground state (S > 0) (*12*).

In the limit of $k_B \cdot T_K \sim \Delta$, both Kondo screening and superconducting pairing are predicted to coexist (*12–14*). Changes in their relative strength can drive the system through a quantum phase transition separating the two different magnetic ground states. Here we experimentally elucidate this competition between pair-breaking and Kondo screening on individual magnetic manganese-phthalocyanine (MnPc) molecules deposited on top of a superconducting Pb(111) substrate. Using scanning tunneling microscopy (STM) and spectroscopy (STS) at 4.5 K, we resolved a complex Kondo fingerprint coexisting with localized bound states within the superconducting gap. On the Pb(111) surface, the MnPc molecule lies in a spin-1 state and is screened by two separate Kondo channels with different strength. The weaker channel competes with the creation of spin-polarized bound states. This competition leads to two different magnetic

Institut für Experimentalphysik, Freie Universität Berlin, Arnimallee 14, 14195 Berlin, Germany.

*To whom correspondence should be addressed. E-mail: franke@physik.fu-berlin.de

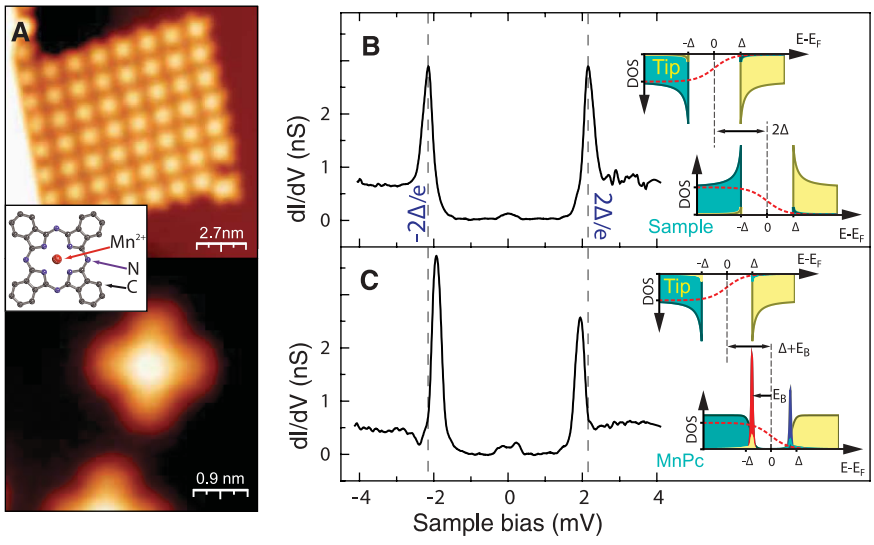

Fig. 1. (**A**) STM image of a densely packed MnPc island and a single molecule (V_s = 200 mV, I = 8.6 pA). (Inset) Molecular structure (*32*). Experimental details are described in SOM 1 (*15*). (**B**) Differential conductance spectrum of the SIS tunneling junction formed by the clean Pb(111) surface and a lead-coated STM tip. Tunneling between quasiparticle peaks of the Bardeen-Cooper-Schrieffer (BCS)–like density of states (DOS) leads to a doubling of the superconducting gap [see SOM 2 (*15*)]. (**C**) The corresponding spectrum on an isolated molecule shows intragap states, which can be related to its magnetic state [corresponding STM image in (A), lower panel].

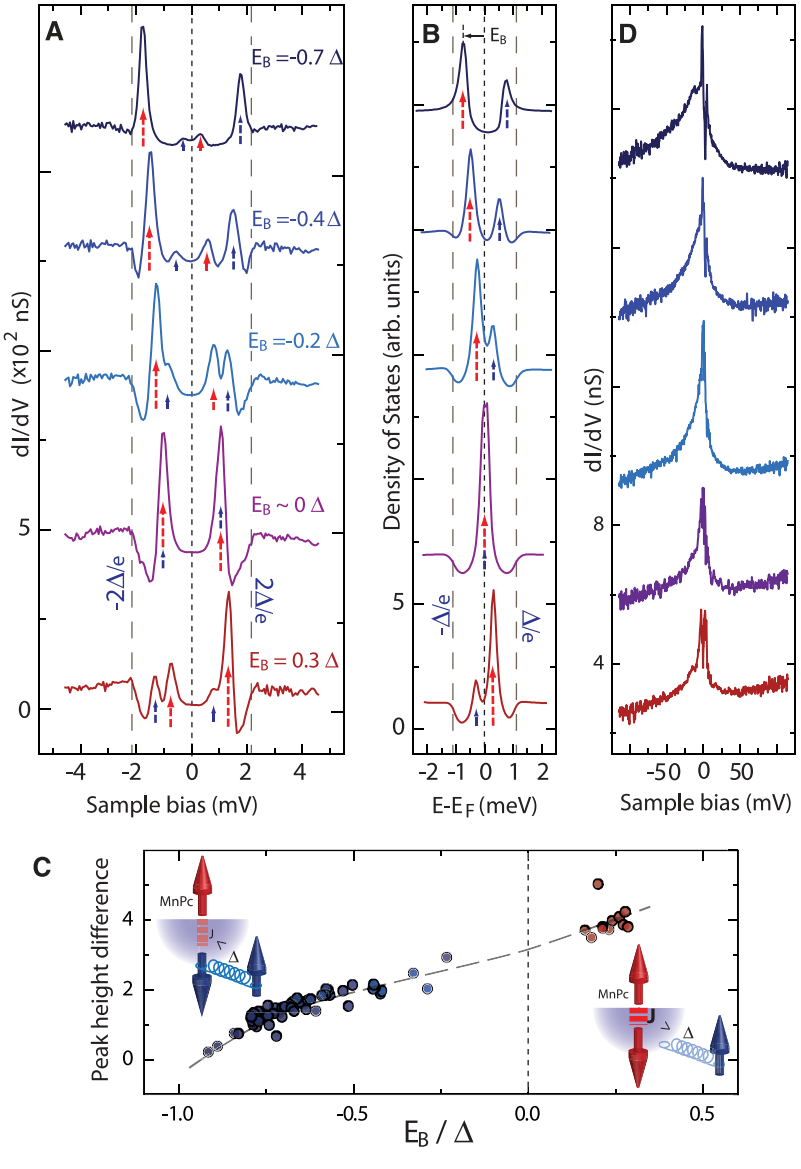

Fig. 2. (**A**) *dI/dV* spectra around the superconducting gap on five characteristic MnPc molecules (feedback opened at V_s = 8.6 mV, I = 0.45 nA; the spectra are shifted for clarity). All of the spectra show that the quasiparticle peaks at $E = \pm 2\Delta$ and the thermal excitation peaks at $E = 0$ are substituted by four peaks inside the superconducting gap: the particle and hole impurity-induced bound states probed by the superconducting tip. The superconducting gap edge, observed in this SIS junction at $\pm 2\Delta$, is indicated with a dashed line. (**B**) Corresponding Mn/Pb(111) DOS obtained by numerical deconvolution of the superconducting tip DOS [SOM 3 (*15*)]. (**C**) The position of the larger bound state E_B is correlated with a monotonous increase in the peak asymmetry, reflecting a continuous gain in its spin polarization at the impurity (the dashed line is added as a guide). Points are omitted near $E_B = 0$ because there both particle- and hole-like states overlap [as shown in (A) and (B)]. The schemes represent the two ground states, a bound Cooper pair ($E_B < 0$) and a bound broken pair ($E_B > 0$). (**D**) Conductance spectra in a larger sample bias window for the same set of molecules as in (A). A broad zero-bias conductance anomaly is revealed, whose specific line shape appears correlated with the alignment of intragap bound states (V_s = 130 mV, I = 0.47 nA).

ground states. In MnPc islands, we observed a transition between the two ground states along a quasi-periodic Moiré pattern, revealing that their different quantum state is tuned by small variations of their interaction with the superconducting substrate. The result is a molecular superstructure wherein superconductivity and magnetism alternate at nanoscopic length scales.

The Pb substrate is a type I superconductor with a critical temperature T_c of 7.2 K. At 4.5 K, the electron density of states is depleted within an energy gap of width $2\Delta = 2.2$ meV around the

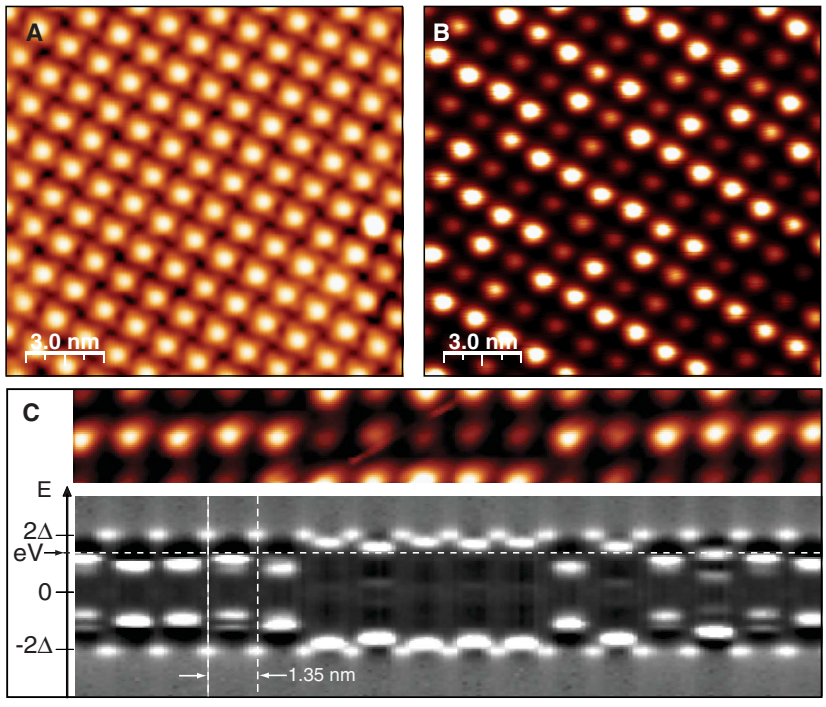

Fig. 3. (**A**) Constant-current STM image of a MnPc island ($V_s = 11$ mV, $I = 27$ pA). (**B**) Corresponding constant-height STM image at $V_s = 1.6$ mV (feedback opened at $V_s = 11$ mV, $I = 27$ pA). A Moiré pattern emerges, revealing that the molecules in the compact islands lie in different adsorption sites with respect to the Pb(111) atomic lattice. (**C**) Current image at constant height of a molecular row of the Moiré pattern and, below, false-color scale *dI/dV* spectra taken along a line crossing through the centers of these molecules. The horizontal dashed line corresponds to the bias value of current images in (B) and (C). Vertical lines point to sites between molecules, where spectra of a bare SIS junction are recovered.

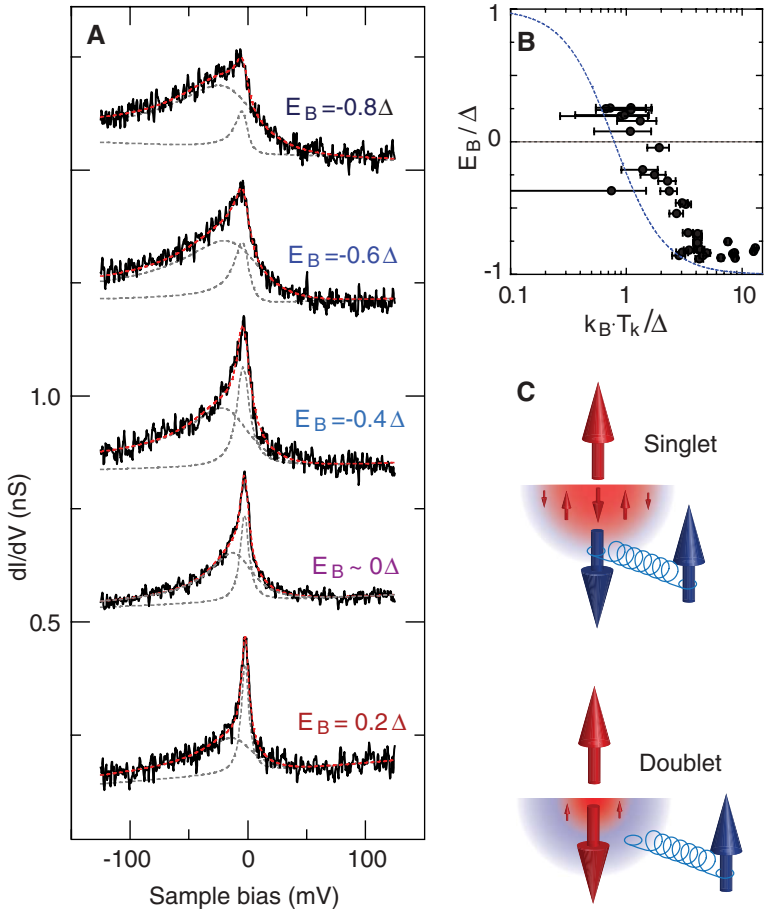

Fig. 4. (**A**) Zero-bias conductance anomalies at 8.8 K (above the T_c of lead) and the resulting fit (dashed red line) using two Fano curves with very different line width (gray dashed lines), representing two screening channels. On the bare Pb(111), flat spectra of a normal metal are obtained (feedback opened at $V_s = 150$ mV, $I = 27$ pA; the spectra are shifted for clarity). (**B**) Relation between the energy scale of the narrower screening channel $k_B \cdot T_K$, obtained at 8.8 K as in (A) (experimental broadening corrected), and the position of the large intragap state E_B, obtained for the same set of MnPc molecules at 4.5 K. The dashed blue line is based on the theory of Matsuura (*13*), modified to simulate the phase transition around $k_B \cdot T_K \sim \Delta$ (*22*, *31*). The weaker the Kondo channel, the larger is the magnetic coupling with superconducting quasiparticles (larger E_B) and the larger is the spin polarization of the total system. (**C**) Simple scheme of the two ground states: a total singlet for $E_B < 0$, formed by a Kondo singlet and a weakly bound Cooper pair; a total doublet for $E_B > 0$, where Kondo screening is incomplete and a broken pair ($s = 1/2$) is bound to the magnetic impurity ($s = 0$).

Fermi energy (E_F). To explore the sub–millielectron volt energy scale in our STS measurements, we used a Pb-coated superconducting tip [see SOM 1 (*15*)]. In this way, the energy resolution is far beyond the limit imposed by the thermal broadening of the Fermi edge of a normal tip [see SOM 2 (*15*)]. The superconductor-insulator-superconductor (SIS) tunnel configuration is revealed in the differential conductance (dI/dV) spectra by two sharp peaks at $\pm 2\Delta = \pm 2.2$ meV, twice the superconducting gap (Fig. 1B), representing the tunneling between the quasiparticle peaks.

MnPc molecules self-assemble in densely packed islands with a square lattice (Fig. 1A). Each molecule is imaged as a fourfold clover-shaped structure with a central protrusion representing the Mn ion. As a reference, we first probe the spectroscopic fingerprint around the E_F of isolated MnPc molecules that were dragged out of the islands with the STM tip. These molecules, all resting on their preferred adsorption site, exhibit similar dI/dV spectra (Fig. 1C) in which the quasiparticle peaks at $\pm 2\Delta$ are substituted by pronounced peaks of asymmetric height within the superconducting gap [at $\pm(E_B + \Delta)$, with $E_B < \Delta$]. The asymmetry between the electron ($V < 0$) and hole-like ($V > 0$) states is an expression of the breaking of time-reversal symmetry by the magnetic interaction between MnPc and Cooper pairs (*2*–*5*, *12*). The close proximity of these new quasiparticle peaks to the superconducting gap edges reflects the rather weak magnetic interaction for these isolated species (*9*, *10*).

The spectra of molecules in the densely packed islands also show molecule-induced bound states, but with a large variety of positions within the energy gap and height asymmetries, depending on the molecule. Figure 2A shows five representative spectra taken on different MnPc molecules. To remove the influence of the superconducting density of states of the tip, we numerically deconvolute its quasiparticle density of states from the dI/dV spectrum [SOM 3 (*15*)]. The resulting plots (Fig. 2B) represent the quasiparticle excitation spectra of the molecule-substrate system with electron and hole-like states at $\pm E_B$ and within the superconducting gap. A shift of the larger (smaller) bound state away from the negative (positive) superconducting gap edge indicates a smaller pairing energy of the Cooper pairs. The decrease in pairing energy is accompanied by an increase in the asymmetry between the peaks of large and small spectral weight as the poles move toward the Fermi level (Fig. 2C) (*9*, *10*, *12*). The crossing of the bound states through the Fermi level ($E_B = 0$) corresponds to the special case when the electron and hole states are degenerate and a quantum phase transition to a different ground state occurs. When the magnetic interaction becomes larger than the pairing energy, the bound Cooper pair is broken (*12*), resulting in a so-called (s = 1/2) Bogoliubov quasiparticle (*5*). This new superconducting ground state is thus characterized by intragap states with larger weight in the hole-like peak (as shown in the lower spectra in Fig. 2, A and B), representing excitations of the (bound) broken pair.

The origin of the different interaction strengths between MnPc molecules and superconducting quasiparticles was determined from an analysis of constant-height current maps of the islands measured at a sample bias $V_s = 1.6$ meV, which is within the superconducting gap (Fig. 3B). In the map, the molecules appear with different brightness, forming a Moiré-like superstructure. A correlation between Moiré pattern and bound states is shown in a series of dI/dV spectra taken along a high-symmetry direction of the superstructure (Fig. 3C). The gray-scale–coded conductance reveals that the bound-state resonances of dark molecules in Fig. 3B lie above the applied bias energy eV_s (similar to the top spectrum in Fig. 2A). Hence, they correspond to MnPc molecules weakly interacting with Cooper pairs. Brighter molecules have bound states below eV_s contributing to the tunneling current and, thus, reveal a larger magnetic interaction with the quasiparticles. Between the molecules, the density of states of the bare SIS junction could be recovered, indicating a very narrow localization of the magnetic bound states (*12*). The Moiré pattern is a geometrical effect, resulting from the quadratic molecular lattice on top of the hexagonal atomic Pb(111) structure [see SOM 4 (*15*)]. Thus, each MnPc molecule is found in a slightly different bonding configuration with the substrate. The direct correlation of the energy alignment of the bound states with the Moiré structure evidences that the magnetic state is strongly influenced by the adsorption site.

We found an additional magnetic fingerprint of the MnPc-lead interaction by exploring dI/dV spectra in a larger energy scale, well outside the superconducting gap. All of the molecules show a pronounced background peak, which has been assigned to tunneling through a Kondo resonance (Fig. 2C) (*16*–*19*). The large energy scale of such zero-bias conductance anomalies revealed that screening of the magnetic molecule by the itinerant electrons of the substrate is very efficient, with T_K roughly between 200 and 400 K, depending on the molecule (*18*, *19*). For such high T_K ($k_B \cdot T_K >> \Delta$), the screening of a spin 1/2 impurity would be complete before the opening of the superconducting energy gap at $T_c = 7.2$ K. This result is in apparent contradiction with the observation of the intragap bound states shown in Fig. 2A. A more complex interpretation of the zero-bias anomaly is needed than one based on a simple spin 1/2 MnPc molecule.

A closer look into the line shape of the background peak reveals that it cannot be simply reproduced by a single Fano function (*18*), as it is characteristic of the Kondo effect. To rule out a distortion of the peak shape by the superconductor bound states, we increased the temperature of the STM to 8.8 K, above the T_c for superconductivity in lead. The spectra maintain their shape, roughly described by a zero-bias sharp peak on top of a wider Fano-like anomaly (Fig. 4A). The best fit to reproduce the resulting plots requires the use of two resonances with very different line widths, representing two different Kondo screening channels, characteristic of a spin-1 system (*20*). The large difference in the energy scales (~1 to 5 meV and ~15 to 45 meV; the exact values depend on the particular molecule in Fig. 2A) of both Kondo processes justifies treating the system as two independent screening channels (*21*).

The energy scale of the narrower Kondo resonance lies in the same range as the superconducting energy gap ($\Delta = 1.1$ meV), thus leading to competing effects in the quasiparticle pairing for temperatures below T_c. Upon opening of the superconducting energy gap, the spin channel becomes underscreened because the density of the itinerant electrons participating in the Kondo screening is depleted. The Kondo screening then competes with magnetically induced bound states like those shown in Fig. 2A. This picture is corroborated in Fig. 4B, where we plot the energy value of the subgap states in the superconducting phase as a function of $k_B \cdot T_K/\Delta$ (i.e., the energy scale of this screening channel). The weaker the Kondo channel, the more strongly bound are the intragap states, qualitatively resembling early theoretical predictions by Matsuura (*13*). According to our results, the crossing of the intragap states through the Fermi level takes place for $k_B \cdot T_K/\Delta \sim 1$ (*22*). At this point, the bounded superconducting quasiparticle goes through a quantum phase transition from a singlet to a doublet ground state (the broken pair). The correlation between T_K and E_B in Fig. 4B further reveals that the screening channel also follows the Moiré pattern shown in Fig. 3. We can then infer that seemingly small changes in adsorption site have an immense impact in the magnetic moment of the underscreened spin (*19*) and, consequently, on the energies of the intragap quasiparticle states.

The observed double Kondo screening can be rationalized considering that the free MnPc molecule lies in a S = 3/2 spin state, with the three unpaired electrons in an electron configuration $(d_{xy})^1(d_\pi)^3(d_{z^2})^1$ (*23*). The interaction of MnPc with the lead surface is rather weak. However, the magnetic moment associated with the d_{z^2} orbital is expected to be quenched (*18*), resulting in a spin-1 system. The double Kondo spectral features are then ascribed to the screening of the two remaining localized spins in the d_{xy} and d_π orbitals, coupled independently with normal electrons of the surface at different energy scales $k_B \cdot T_K$. The broader Kondo channel, with T_K ~200 to 400 K (*24*), fully screens the magnetic moment of one of the orbitals. The other orbital is only partially screened by the low-energy Kondo channel, thus interacting with superconducting quasiparticles depending on the commensuration with the lead atomic lattice underneath. The resulting quantum state of the complete system is a singlet or doublet (Fig. 4C),

depending on the particle or hole character of the larger intragap state, respectively. Such different quantum systems coexist and alternate between neighboring molecules because of their high localization at the impurity site.

The MnPc molecular superstructure thus represents a useful nanoscopic workbench where magnetic coupling with the substrate can be measured from the alignment of the bound states and tuned by choosing the appropriate molecule. The interaction of these bound states with other intragap excitations [e.g., multiple Andreev reflections in contact junctions (*25*–*27*)] or with superconductors with other symmetries [e.g., p-wave (*28*–*30*)] represents a fascinating application of this study to ongoing problems in condensed-matter physics.

References and Notes

1. J. Kondo, *Prog. Theor. Phys.* **32**, 37 (1964).
2. L. Yu, *Acta Phys. Sin.* **21**, 75 (1965).
3. H. Shiba, *Prog. Theor. Phys.* **40**, 435 (1968).
4. A. I. Rusinov, *Zh. Eksp. Teor. Fiz.* **56**, 2047 (1969) [*Sov. Phys. JETP* **29**, 1101 (1969)].
5. A. V. Balatsky, I. Vekhter, J.-X. Zhu, *Rev. Mod. Phys.* **78**, 373 (2006).
6. A. Yazdani, B. A. Jones, C. P. Lutz, M. F. Crommie, D. M. Eigler, *Science* **275**, 1767 (1997).
7. S.-H. Ji *et al.*, *Phys. Rev. Lett.* **100**, 226801 (2008).
8. C. P. Moca, E. Demler, B. Janko, G. Zarand, *Phys. Rev. B* **77**, 174516 (2008).
9. M. E. Flatté, J. M. Byers, *Phys. Rev. B* **56**, 11213 (1997).
10. M. Flatté, J. Byers, *Phys. Rev. Lett.* **78**, 3761 (1997).
11. M. R. Buitelaar, T. Nussbaumer, C. Schönenberger, *Phys. Rev. Lett.* **89**, 256801 (2002).
12. M. I. Salkola, A. V. Balatsky, J. R. Schrieffer, *Phys. Rev. B* **55**, 12648 (1997).
13. T. Matsuura, *Prog. Theor. Phys.* **57**, 1823 (1977).
14. O. Sakai, Y. Shimizu, H. Shiba, K. Satori, *J. Phys. Soc. Jpn.* **62**, 3181 (1993).
15. Materials and methods are available as supporting material on *Science* Online.
16. V. Madhavan V, W. Chen, T. Jamneala, M. F. Crommie, N. S. Wingreen, *Science* **280**, 567 (1998).
17. J. Li, W.-D. Schneider, R. Berndt, B. Delley, *Phys. Rev. Lett.* **80**, 2893 (1998).
18. Y.-S. Fu *et al.*, *Phys. Rev. Lett.* **99**, 256601 (2007).
19. S.-H. Ji *et al.*, *Chin. Phys. Lett.* **27**, 087202 (2010).
20. J. J. Parks *et al.*, *Science* **328**, 1370 (2010).
21. A. Posazhennikova, P. Coleman, *Phys. Rev. Lett.* **94**, 036802 (2005).
22. The crossing point differs from the estimated value $k_B \cdot T_K/\Delta \sim 0.3$ (*13*, *14*). Recent renormalization group theory calculations find that the quantum phase transition may vary depending on the parameters (*31*). We note that the more complex double Kondo state of MnPc may influence the transition.
23. M.-S. Liao, J. D. Watts, M.-J. Huang, *Inorg. Chem.* **44**, 1941 (2005).
24. L. Gao *et al.*, *Phys. Rev. Lett.* **99**, 106402 (2007).
25. M. Ternes *et al.*, *Phys. Rev. B* **74**, 132501 (2006).
26. A. Eichler *et al.*, *Phys. Rev. Lett.* **99**, 126602 (2007).
27. T. Sand-Jespersen *et al.*, *Phys. Rev. Lett.* **99**, 126603 (2007).
28. G. E. Volovik, *JEPTP Lett.* **70**, 609 (1999).
29. N. Read, D. Green, *Phys. Rev. B* **61**, 10267 (2000).
30. D. A. Ivanov, *Phys. Rev. Lett.* **86**, 268 (2001).
31. J. Bauer, A. Oguri, A. C. Hewson, *J. Phys. Condens. Matter* **19**, 486211 (2007).
32. I. Horcas *et al.*, *Rev. Sci. Instrum.* **78**, 013705 (2007).

Acknowledgments: We thank F. von Oppen and A. Strozecka for stimulating discussions and E.K.U. Gross for motivating us to study this topic. This research was supported by the Focus area "Nanoscale Materials" of the Freie Universität Berlin and by the Deutsche Forschungsgemeinschaft through the collaborative projects Sfb 658 and SPP 1243.

Supporting Online Material

www.sciencemag.org/cgi/content/full/332/6032/940/DC1
Materials and Methods
Figs. S1 to S4

27 December 2010; accepted 6 April 2011
10.1126/science.1202204

Chlorinated Indium Tin Oxide Electrodes with High Work Function for Organic Device Compatibility

M. G. Helander,[1*†] Z. B. Wang,[1*†] J. Qiu,[1] M. T. Greiner,[1] D. P. Puzzo,[1] Z. W. Liu,[1*] Z. H. Lu[1,2*]

In organic light-emitting diodes (OLEDs), a stack of multiple organic layers facilitates charge flow from the low work function [~4.7 electron volts (eV)] of the transparent electrode (tin-doped indium oxide, ITO) to the deep energy levels (~6 eV) of the active light-emitting organic materials. We demonstrate a chlorinated ITO transparent electrode with a work function of >6.1 eV that provides a direct match to the energy levels of the active light-emitting materials in state-of-the art OLEDs. A highly simplified green OLED with a maximum external quantum efficiency (EQE) of 54% and power efficiency of 230 lumens per watt using outcoupling enhancement was demonstrated, as were EQE of 50% and power efficiency of 110 lumens per watt at 10,000 candelas per square meter.

Transparent tin-doped indium oxide (ITO) electrodes are used in several classes of devices, including liquid crystal displays, organic photovoltaics, and organic light-emitting diodes (OLEDs) (*1*–*11*). Despite the dominance of ITO in the flat-panel display industry, its surface electronic properties are less than ideal for organic devices. In particular, the low work function of ITO complicates the design of organic optoelectronic devices in terms of charge injection from the electrodes because of the large mismatch between the low work function of ITO (~4.7 eV) and the energy levels of the active organic materials used in devices (*12*, *13*) (typically 5.7 to 6.3 eV). For example, the highest occupied molecular orbital (HOMO) of commonly used host materials in state-of-the-art phosphorescent OLEDs is typically ~6 eV, which is much too deep to directly inject charge from ITO.

As a result, multiple transport layers are required to match the energy levels in a stepwise fashion. An additional injection layer is also typically used, with the most common examples being copper phthalocyanine (*14*), poly(3,4-ethylenedioxythiophene) (PEDOT) (*15*), transition-metal oxides (*16*), or p-doped organic layers (*17*–*19*). Each additional layer that is required greatly increases the manufacturing costs and also introduces additional hetero-junctions into the device that can be detrimental to device stability and performance (*20*, *21*). A transparent electrode with a tunable high work function that matches the energy levels of the active organic material would avoid the requirement for multiple transport and injection layers.

To address this issue, we functionalized the surface of ITO with a controlled amount of electronegative halogen atoms that were derived from an inert halogenated solvent precursor that was activated with ultraviolet (UV) radiation. An air-stable electrode with a work function greater than 6.1 eV was achieved in the case of chlorinated ITO (Cl-ITO) without altering the surface roughness, transparency, and conductivity of the electrode. The tunable high work function enabled the fabrication of a highly simplified OLED with a high efficiency and brightness.

To fabricate Cl-ITO, we placed bare substrates in a closed Pyrex reaction vessel with *o*-dichlorobenzene and treated them with UV radiation from a low-pressure mercury lamp (SEN Lights PL16-110) for up to 10 min [see (*22*) for details]. Cl radicals liberated from the solvent displaced oxygen on the surface of the electrode. After treatment with UV radiation, the substrates were exposed to UV-generated ozone for an additional 3 min to fully oxidize any residual chlorocarbon fragments on the surface (fig. S3). X-ray photoelectron spectroscopy (XPS) was used to characterize the work function and surface composition of the Cl-ITO electrode. The secondary electron cut-off of Cl-ITO as a function of increasing UV treatment time from 0 to 10 min monotonically shifted to lower binding energy, indicating an increase in work function (Fig. 1A). The intensity of the Cl 2p peak (Fig. 1B)

[1]Department of Materials Science and Engineering, University of Toronto, 184 College Street, Toronto, Ontario, Canada M5S 3E4. [2]Department of Physics, Yunnan University, 2 Cuihu Beilu, Yunnan, Kunming 650091, People's Republic of China.

*To whom correspondence should be addressed. E-mail: michael.helander@utoronto.ca (M.G.H.); zhibin.wang@utoronto.ca (Z.B.W.); zhiwei.liu@utoronto.ca (Z.W.L); zhenghong.lu@utoronto.ca (Z.H.L)
†These authors contributed equally to this work.